



HAL
open science

Conductance-based phenomenological non-spiking model: a dimensionless and simple model that reliably predicts the effects of conductance variations on non-spiking neuronal dynamics

Loïs Naudin, Laetitia Raison-Aubry, Laure Buhry

► **To cite this version:**

Loïs Naudin, Laetitia Raison-Aubry, Laure Buhry. Conductance-based phenomenological non-spiking model: a dimensionless and simple model that reliably predicts the effects of conductance variations on non-spiking neuronal dynamics. 2022. hal-03778396

HAL Id: hal-03778396

<https://hal.science/hal-03778396>

Preprint submitted on 15 Sep 2022

HAL is a multi-disciplinary open access archive for the deposit and dissemination of scientific research documents, whether they are published or not. The documents may come from teaching and research institutions in France or abroad, or from public or private research centers.

L'archive ouverte pluridisciplinaire **HAL**, est destinée au dépôt et à la diffusion de documents scientifiques de niveau recherche, publiés ou non, émanant des établissements d'enseignement et de recherche français ou étrangers, des laboratoires publics ou privés.

1 Conductance-based phenomenological non-spiking
2 model: a dimensionless and simple model that reliably
3 predicts the effects of conductance variations on
4 non-spiking neuronal dynamics

5 Loïs Naudin^{1**}, Laetitia Raison-Aubry¹⁺, and Laure Buhry¹

6 ¹Laboratoire Lorrain de Recherche en Informatique et ses Applications,
7 CNRS, Université de Lorraine, Nancy, France

8 *Corresponding author: lois.naudin@gmail.com

9 ⁺These authors contributed equally (joint first author)

10 September 13, 2022

11 **Abstract**

12 The modeling of single neurons has proved to be an indispensable tool in decipher-
13 ing the mechanisms underlying neural dynamics and signal processing. In that sense,
14 two types of single-neuron models are extensively used: the conductance-based mod-
15 els (CBMs) and the so-called ‘phenomenological’ models, which are often opposed in
16 their objectives and their use. Indeed, the first type aims to describe the biophysical
17 properties of the neuron cell membrane that underlie the evolution of its potential,
18 while the second one describes the macroscopic behavior of the neuron without taking
19 into account all its underlying physiological processes. Therefore, CBMs are often
20 used to study ‘low-level’ functions of neural systems, while phenomenological models
21 are limited to the description of ‘high-level’ functions. In this paper, we develop a
22 numerical procedure to endow a dimensionless and simple phenomenological non-
23 spiking model with the capability to describe the effect of conductance variations on
24 non-spiking neuronal dynamics with high accuracy. The procedure allows to deter-
25 mine a relationship between the dimensionless parameters of the phenomenological

26 model and the maximal conductances of CBMs. In this way, the simple model com-
27 bines the biological plausibility of CBMs with the high computational efficiency of
28 phenomenological models, and thus may serve as a building block for studying both
29 ‘high-level’ and ‘low-level’ functions of non-spiking neural networks.

30
31 **Keywords:** Simple neuron model; non-spiking neurons; conductance variations;
32 bifurcation; *Caenorhabditis elegans*; retina.

33 1 Introduction

34 To better understand how neuronal circuits control behavior and brain functions, neuron
35 modeling is a widely-used tool. Two types of models characterizing the dynamics of sin-
36 gle neurons can be used. The first one is the conductance-based model (CBM), which
37 inherits the Hodgkin-Huxley formalism (Hodgkin and Huxley, 1952) and aims to describe
38 the biophysical properties of the neuron cell membrane that underlie the evolution of its
39 potential. In this model, every individual parameter and state variable has an established
40 electrophysiological meaning. Therefore, CBMs are broadly used to understand ‘low-level’
41 functions of neural systems (Eliasmith and Trujillo, 2014; O’Leary et al., 2015), such as
42 monitoring the effects of specific conductance variations on neuronal dynamics (Giovannini
43 et al., 2017; Poirazi and Papoutsis, 2020), or modeling gain- or loss-of-function mutations
44 in genes encoding ion channels (Lemaire et al., 2021).

45 The second type of model is often qualified by the term ‘phenomenological’, although
46 some authors contradict it (Brette, 2015). This type of model was developed in part to
47 overcome the drawbacks of CBMs, which are twofold: (i) they have a very high computa-
48 tional cost due to their complexity so that only a handful of neurons can be simulated in
49 real time (Izhikevich, 2004), and (ii) the insights obtained from a mathematical analysis
50 are quite limited as these are high-dimensional systems (Ermentrout and Terman, 2010).
51 A phenomenological model therefore aims to be lightweight, simple, and to describe the
52 macroscopic behavior of the neuron without taking into account all its underlying physi-
53 ological processes. Some classical examples are the FitzHugh–Nagumo model (FitzHugh,
54 1961), Izhikevich model (Izhikevich, 2003), or many integrate-and-fire models (Latham
55 et al., 2000; Smith et al., 2000; Górski et al., 2021). The counterpart of phenomenological
56 models is that their parameters are dimensionless, thus limited to the study of ‘high-level’
57 functions of neural systems.

58 A simple phenomenological model of non-spiking neurons was recently developed in
59 Naudin et al. (2022b). This type of neuron is found in a wide variety of nervous tissues

60 (Davis and Stretton, 1989b; Goodman et al., 1998; Field and Chichilnisky, 2007), encodes
61 neuronal information in an analog manner through graded responses (Lockery et al., 2009),
62 and plays a crucial role in the functioning of many nervous systems (Roberts and Bush,
63 1981; Burrows et al., 1988; Laurent and Burrows, 1989; Davis and Stretton, 1989a; Bidaye
64 et al., 2018). Further, three phenotypes of non-spiking neurons can be distinguished (Fig-
65 ure S2), each with its own computational properties (Naudin et al., 2022c): (i) near-linear,
66 defined by smooth depolarizations or hyperpolarizations from the resting potential (pheno-
67 type 1), (ii) bistable, characterized by nonlinear transitions between the resting potential
68 and a depolarized potential, with one resting potential (phenotype 2), and (iii) bistable
69 with two resting potentials (phenotype 3). Naudin et al. (2022c) described a general pat-
70 tern of the phenotypic evolution of non-spiking neurons as a function of changes in calcium
71 and potassium conductances. As an example, Figure 1 illustrates the phenotypic transi-
72 tions of non-spiking neurons as calcium conductance (g_{Ca}) decreases through a well-posed
73 retinal cone non-spiking CBM (Kourennyi et al., 2004). To sum up, the wild-type CBM
74 endowed with a phenotype 3 switches to a phenotype 2 and then 1 as g_{Ca} decreases.

75 The aim of this paper is the development of a numerical procedure to determine a
76 relationship between the dimensionless parameters of the phenomenological non-spiking
77 model (Naudin et al., 2022b) and the calcium conductance of a non-spiking cell, in order
78 to reproduce its phenotypic transitions as g_{Ca} decreases (Figure 1). In other words, the
79 dimensionless parameters of the simple model are expressed as a function of g_{Ca} . In
80 this way, our resulting simple model, called ‘conductance-based phenomenological non-
81 spiking model’, combines the biological plausibility of CBMs with the high computational
82 efficiency of phenomenological models, and thus may serve as a building block for studying
83 both ‘high-level’ and ‘low-level’ functions of non-spiking neural networks. To illustrate our
84 method, the procedure is applied to a model of an intrinsically non-spiking cell type, the
85 retinal cone.

86 The remainder of the paper is organized as follows. Section 2 describes the evolution
87 of the computational characteristics of the retinal cone CBM as g_{Ca} decreases, that is
88 representative of an ubiquitous and general pattern in non-spiking neurons (Naudin et al.,
89 2022c). Section 3 proposes a numerical procedure to build a phenomenological model
90 that reproduces the computational characteristic evolution of the retinal cone CBM as g_{Ca}
91 reduces, as described in Section 2. Then, we analyse in Section 4 the dynamics of the
92 resulting model and show that it is well-suited to characterize the phenotypic evolution of
93 the neuron as g_{Ca} decreases. Finally, Section 5 discusses the implications on the modeling
94 of the retina and *C. elegans* networks which are two non-spiking nervous tissues.

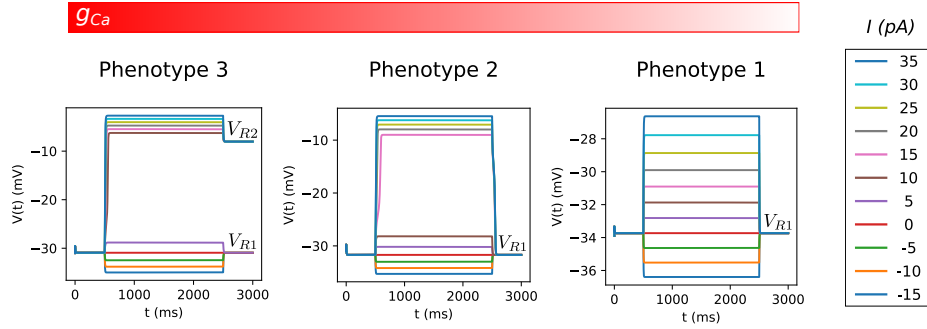


Figure 1: **Phenotypic transitions of the voltage dynamics as g_{Ca} decreases (Naudin et al., 2022c).** A well-posed retinal cone model, with a wild-type phenotype 3, was used as an illustration. A neuron with such a phenotype displays two resting potential values (V_{R1} and V_{R2}). Decreasing g_{Ca} changes the voltage dynamics of the neuron which becomes bistable with only one resting potential (phenotype 2). Finally, the even greater decrease of g_{Ca} leads to the loss of the bistability of the neuron which becomes near-linear (phenotype 1).

2 Preliminaries: evolution of the non-spiking neuron computational characteristics as g_{Ca} decreases

A previous work (Naudin et al., 2022c) determined an ubiquitous and general pattern of non-spiking neuron dynamics as g_{Ca} decreases, illustrated through a well-posed retinal cone CBM (described in Supplementary materials) in Figure 1. It consists in a transition from phenotype 3 to 2 and then to 1 as g_{Ca} decreases. This section aims at describing the computational implications of this phenotypic evolution on the dynamics of the CBM under study.

The evolution of the computational characteristics of a non-spiking CBM can be inferred from the evolution of its steady-state current (SSC). Indeed, the SSC is the underlying data that confers *all* the qualitative neuro-computational characteristics to non-spiking neurons (Naudin et al., 2022a). Thus, we show in Figure 2.A the evolution of the SSC of the CBM under study as g_{Ca} decreases. The wild-type (WT) SSC ($g_{Ca} = 4.92\text{nS}$) exhibits a region with negative slope that becomes less and less steep and then disappears as g_{Ca} decreases. This evolution is due to a counterbalanced flow of I_{Ca} and I_K that underlies the negative slope in the SSC of the neuron (Naudin et al., 2022c). This specific voltage-dependence of membrane current is a common mechanism across the animal phyla, including *C. elegans* neurons (Goodman et al., 1998; Mellem et al., 2008; Nicoletti et al., 2019), vertebrate retina cells (Kourennyi et al., 2004; Aoyama et al., 2000; Usui et al., 1996), vertebrate hair

114 cells (Art and Goodman, 1996; Fettiplace, 1987) and thalamocortical neurons (Hughes
115 et al., 1999; Williams et al., 1997). Therefore, the evolution of the SSC under the effect of
116 decreasing g_{Ca} shown in Figure 2.A is representative of a general pattern. This evolution
117 implies a qualitative change in the computational characteristics of non-spiking neurons
118 that we discuss now.

119 The wild-type SSC ($g_{Ca} = 4.92\text{nS}$) is N-shaped with two stable zeros (phenotype 3).
120 This provides the neuron with two resting potentials, which gives it a short-term memory
121 capacity: the response of the cell depends on its recent history of activity by storing
122 information about its last input (Figure 2.B). For detailed explanations from a dynamical
123 system viewpoint about the mechanism underlying this phenomenon, we refer to Figure
124 S3 and Naudin et al. (2022c). Then, the negative slope of the SSC becomes less and
125 less steep as g_{Ca} decreases (Figure 2.A), until its local minima becomes positive (*e.g.*,
126 $g_{Ca} = 4.22\text{nS}$). Therefore, the neuron is still bistable but with only one resting potential
127 (phenotype 2). This implies that the neuron has lost its short-term memory capacity, so
128 the cell’s response no longer reflects the history of its inputs and of its activity (Figure
129 2.C). Finally, an even more decreased value of g_{Ca} (*e.g.*, $g_{Ca} = 2.02\text{nS}$) gives a monotonic
130 SSC: the neuron becomes near-linear. To sum up, the wild-type neuron with phenotype
131 3 switches to a phenotype 2, and then from 2 to 1 as g_{Ca} decreases. In other words, the
132 neuron first loses its short-term memory capacity (transition from phenotype 3 to 2), then
133 loses its bistable behavior to a near-linear one (transition from phenotype 2 to 1). One
134 last important evolution of the computational characteristics of the neuron as g_{Ca} reduces
135 is the decrease of the voltage amplitude (Figure 2.D).

136 The aim of the following section is to propose a procedure that endows a recent and
137 novel non-spiking phenomenological model with the capability to reproduce the evolution
138 of these computational characteristics of the retinal cone CBM as g_{Ca} varies.

139 **3 Design procedure of the conductance-based phe-** 140 **nomenological non-spiking model**

141 This section aims at proposing a methodology to build a simple and lightweight model that
142 reproduces the qualitative evolution of non-spiking neuron dynamics as g_{Ca} decreases, as
143 described in the previous section. The simple model, described in Materials and methods,
144 has the advantage of having a very low computational cost so that one can simulate large-
145 scale neuronal networks in real time (Naudin et al., 2022b), which is more difficult with
146 CBMs due to their complexity (Izhikevich, 2004). Moreover, the simplicity of this model

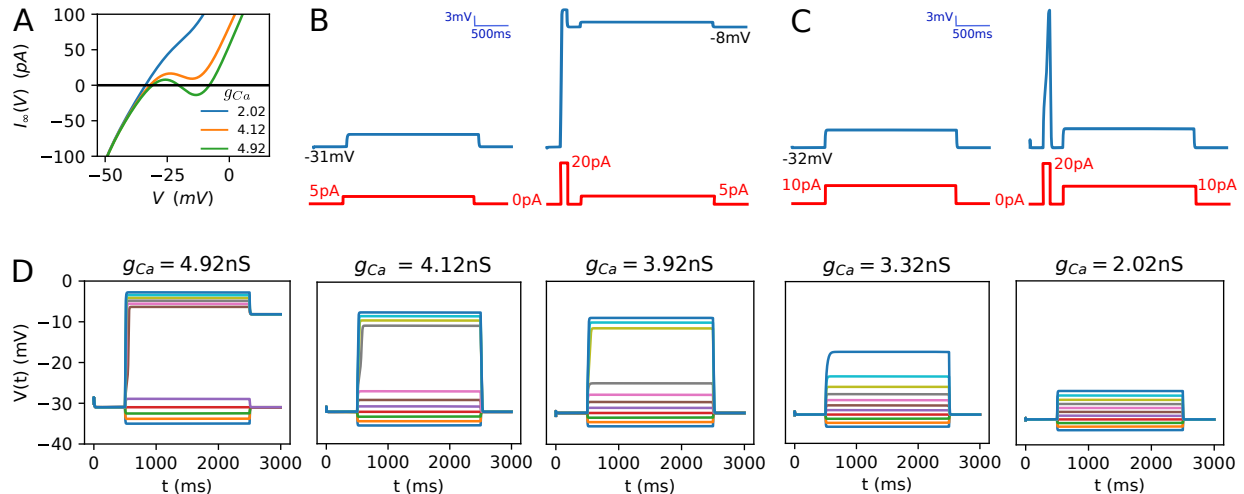


Figure 2: **Evolution of the computational characteristics of the retinal cone CBM as g_{Ca} decreases.** (A) SSC curve for three different values of g_{Ca} (4.92 (WT), 4.12, 2.02). (B) Short-term memory capacity of the WT phenotype of the CBM (phenotype 3). (Left) A depolarizing current step (5pA) of 2000ms duration into the neuron is applied. On cessation of the current step, the voltage stabilizes at its lower resting potential (about -31mV). (Right) A high transient pulse (20pA) of 100ms duration is first injected into the neuron. Its membrane potential then relaxes to its highest resting potential value (approximately -8mV), and finally stabilizes at about -6mV in response to the same current injection protocol as before (current injection step at 5pA under 2000ms). (C) Response of the neuron with a reduced value of g_{Ca} ($g_{Ca} = 4.22$ nS). Whatever the stimulation protocol used, the neuron stabilizes at a steady-state value of about -29mV: the response of the neuron no longer reflects the history of its inputs. (D) Decrease of the voltage amplitude as g_{Ca} decreases, for a series of current injections starting from -15pA and increasing to 35pA by 5pA increments.

147 allows a theoretical mathematical analysis to gain insight into neuronal dynamics (Naudin,
 148 2022). Thus, this section proposes a methodology to build such a simple model that reliably
 149 predicts the effects of calcium conductance variations on the neuron dynamics. In this way,
 150 the model would combine a high computational efficiency and simplicity of mathematical
 151 analysis, with the biological plausibility of CBMs.

152 The methodology is based on the fitting of the evolution of the SSC as g_{Ca} decreases
 153 since it determines the neuro-computational features of a non-spiking neuron, as explained
 154 above. The fitting of the SSCs by the cubic function

$$f(V) = aV^3 + bV^2 + cV + d \quad (1)$$

155 of the simple model is based on the Lagrange interpolation theorem. This theorem gives
 156 unique combinations of parameters (a, b, c, d) for which the third-degree polynomial f
 157 passes through any four given points. Therefore, the aim is to consider four specific points
 158 of the SSC to be interpolated by f . Figure 3 shows the two general steps of the procedure,
 159 that we apply to the CBM under study in the case of g_{Ca} . The detail of the procedure is
 160 given below.

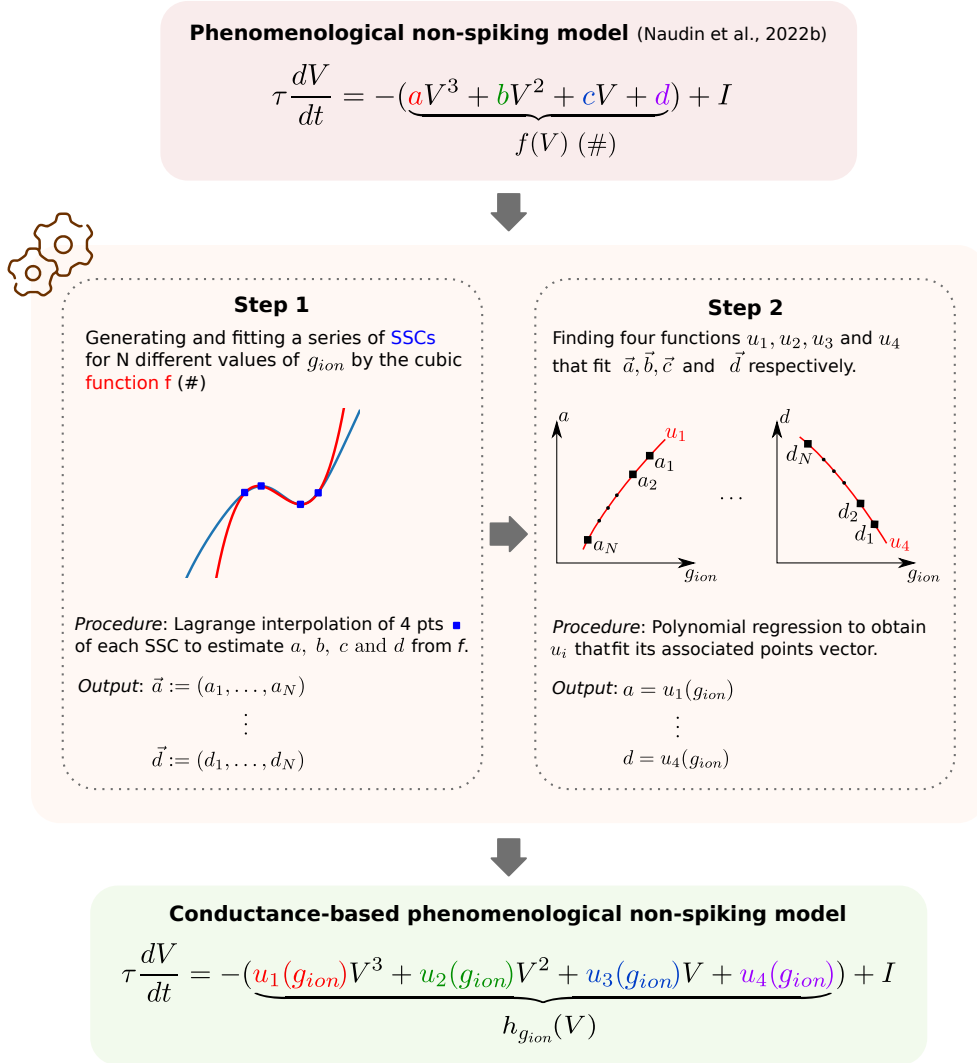


Figure 3: **Overview of the model design procedure.** **(Top)** The phenomenological non-spiking model (Naudin et al., 2022b) comprises 4 dimensionless parameters a , b , c and d . **(Middle)** The two-stage procedure aims to find a relationship between these parameters and maximal conductances g_{ion} of neurons or CBMs. **(Bottom)** After applying the procedure, the conductance-based phenomenological non-spiking model is obtained and depends only on the g_{ion} parameter.

161 • **Step 1a.** Reproducing the wild-type SSC of the neuron by the cubic function f (1):
 162 **Procedure:** To fit the wild-type SSC of the neuron ($g_{Ca} = 4.92\text{nS}$ in our case), we
 163 need to consider four points to be interpolated by the cubic function f . Based on
 164 the previous section, the four points of the SSC that play a paramount role in the
 165 dynamics of the neuron of phenotype 3 are the following:

- 166 – *Resting potentials:* The two stable zeros of the SSC curve, *i.e.* the resting
 167 potentials (red points in Figure 4.A).
- 168 – *Local minima and maxima of the SSC:* The local minima and maxima of the SSC
 169 curve (blue points in Figure 4.A) because they determine the current injection
 170 thresholds at which the voltage jumps to a new plateau.

171 Therefore, the parameters (a, b, c, d) of the function f are determined through La-
 172 grange interpolation so that f passes through these four points.

173 **Output:** One vector of parameters (a, b, c, d) for which the cubic function $f(V) =$
 174 $aV^3 + bV^2 + cV + d$ interpolates the four fundamental points of the SSC of the CBM
 175 (V_{R1} , V_{R2} and the local minima and maxima of the SSC curve)

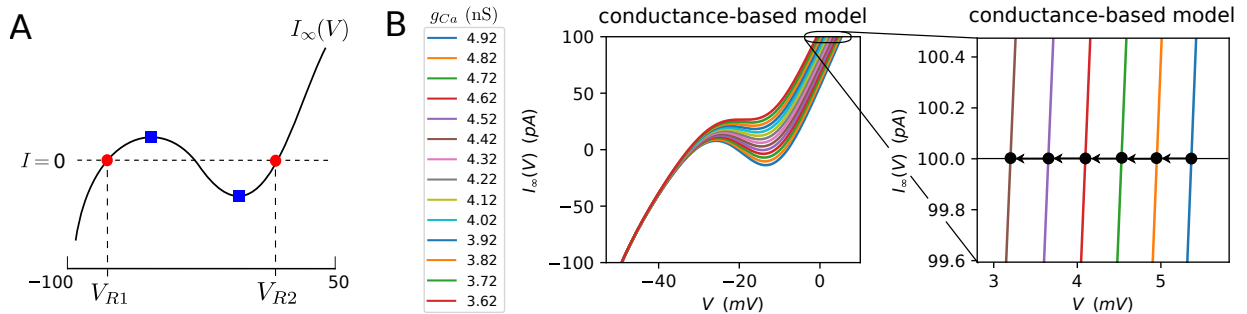


Figure 4: (A) The four points of the wild-type SSC to be interpolated by the cubic function of the simple model. Blue squares denote the local minima and maxima of the SSC, representing the current injection thresholds at which the neuron jumps to a new voltage plateau. Red points denote the two stable zeros of the SSC, representing the two resting potentials of the neuron. (B) The V -coordinate of the upper bound (100pA) of the SSC of the CBM decreases more and more as g_{Ca} decreases, which implies a decrease of the voltage amplitude of the neuron as g_{Ca} decreases. The cubic function f of the simple model will then reproduce this pattern in its upper bound.

176 • **Step 1b.** Generating four points of the SSC to be interpolated for a series of g_{Ca}
 177 associated with phenotypes 3 and 2 by 0.1nS decrements:

178 **Procedure:** The SSC for phenotypes 3 and 2 is N-shaped (Figure 2.A). Then, the

four points for interpolation by the function f are the local minima and maxima of the SSC curve, and the two points of the lower and upper bounds (-100pA and 100pA respectively in this paper):

- *Local minima and maxima of the SSC:* For each SSC of the CBM generated with a new value of g_{Ca} associated with phenotypes 3 and 2, we compute its local minima and maxima, as in Step 1. For the CBM under study, we consider $g_{Ca} \in \{4.82, 4.72, \dots, 3.62\}$.
- *Upper bound of the SSC:* As can be seen in Figure 4.B, the V -coordinate of the upper bound of the SSC of the CBM decreases more and more as g_{Ca} decreases. This implies the decrease in voltage magnitude as g_{Ca} decreases, a paramount computational feature of the CBM shown in the previous section. To endow the simple model with this characteristic, we generate points in the upper bound that decrease in the V -coordinate in a recursive way from the cubic curve obtained in Step 1.
- *Lower bound of the SSC:* As can be seen in Figure 4, the V -coordinate of the lower bound of the SSC of the CBM remains relatively constant. The cubic function f will seek to preserve such a characteristic.

Output: A series of vector points $\vec{a} := (a_{4.92}, a_{4.82}, \dots, a_{3.62})$, $\vec{b} := (b_{4.92}, b_{4.82}, \dots, b_{3.62})$, $\vec{c} := (c_{4.92}, c_{4.82}, \dots, c_{3.62})$, and $\vec{d} := (d_{4.92}, d_{4.82}, \dots, d_{3.62})$.

- **Step 2.** Fitting independently the points of \vec{a} , \vec{b} , \vec{c} , and \vec{d} obtained in Step 2:

Procedure: Finding four functions u_1 , u_2 , u_3 and u_4 that verify $a = u_1(g_{Ca})$, $b = u_2(g_{Ca})$, $c = u_3(g_{Ca})$ and $d = u_4(g_{Ca})$. In this way, we establish a direct relationship between the parameters a , b , c , and d of the simple model and the calcium conductance g_{Ca} of the CBM. To that end, the functions u_1 , u_2 , u_3 and u_4 are considered as polynomials so that polynomial regressions are performed to fit the points of \vec{a} , \vec{b} , \vec{c} and \vec{d} , respectively. We stress the importance to choose polynomials that are not too complex, *i.e.* with degrees that are not too high. Indeed, the SSCs for the phenotype 1 are generated from these functions, *i.e.* for novel values of g_{Ca} not considered during the building of u_1 , u_2 , u_3 and u_4 through the polynomial regression processes. Therefore, the polynomials should not be too complex to avoid an overfitting of data points which would lead to an inability of the model to generate adequate SSCs for phenotypes 1. In our case, two-degree polynomials u_1 , u_2 , u_3 and u_4 will be sufficient to obtain good results (see next section).

Input: Vector points $\vec{a} = (a_{4.92}, a_{4.82}, \dots, a_{3.62})$, $\vec{b} = (b_{4.92}, b_{4.82}, \dots, b_{3.62})$,

213 $\vec{c} = (c_{4.92}, c_{4.82}, \dots, c_{3.62})$, and $\vec{d} = (d_{4.92}, d_{4.82}, \dots, d_{3.62})$.

214 **Output:** Four functions u_1 , u_2 , u_3 , and u_4 that verify $a = u_1(g_{Ca})$, $b = u_2(g_{Ca})$,
 215 $c = u_3(g_{Ca})$ and $d = u_4(g_{Ca})$, such as we obtain the new model:

$$\tau \frac{dV}{dt} = -h_{g_{Ca}}(V) + I \quad (2)$$

216 with

$$h_{g_{Ca}}(V) := u_1(g_{Ca})V^3 + u_2(g_{Ca})V^2 + u_3(g_{Ca})V + u_4(g_{Ca}). \quad (3)$$

217 so that the simple model (2) depends only on the calcium conductance parameter.

218 In the next section, we show and discuss the results obtained from the procedure pro-
 219 posed in this section applied to the CBM under study.

220 4 Analysis of the model dynamics

221 A procedure to build a simple model that reproduces the qualitative evolution of non-
 222 spiking neuron dynamics as g_{Ca} evolves has been proposed in the previous section. Since
 223 the qualitative evolution of non-spiking neuron dynamics as g_{Ca} evolves is reflected by the
 224 evolution of the SSC, the procedure consists in reproducing this evolution of the SSC by
 225 the function $h_{g_{Ca}}$ of the model (2). The result of this procedure is shown in Figure 5
 226 which we compare the evolution of the SSC of the CBM with the function h (Eq. (3)) for
 227 different values of g_{Ca} , starting from 4.92nS and decreasing to 0.02nS by 0.2nS decrements.
 228 The interpolation functions u_i , $i = 1, \dots, 4$, of the function h are shown in Figure S4. In
 229 particular, we can observe in Figure 5 that the qualitative evolution of the SSC as g_{Ca}
 230 decreases is reproduced with a high fidelity by the cubic function. The purpose of this
 231 section is to discuss the implications on the resulting voltage dynamics.

232 The first important implication is the occurrence of transitions between different phe-
 233 notypes for the same g_{Ca} values in the CBM as in the simple model. Indeed, the transition
 234 between phenotype 3 and 2 occurs at $g_{Ca} = 4.50$ nS, both in the CBM and in the simple
 235 model. In other words, the CBM and the simple model lose their short-term memory ca-
 236 pacity at the same g_{Ca} value. Similarly, the transition between phenotype 2 and 1 occurs
 237 at $g_{Ca} = 3.59$ nS in the CBM, and at $g_{Ca} = 3.50$ nS in the simple model. Therefore, the loss
 238 of bistability in favor of a near-linear type behavior occurs at about the same g_{Ca} values
 239 in the CBM as in the simple model.

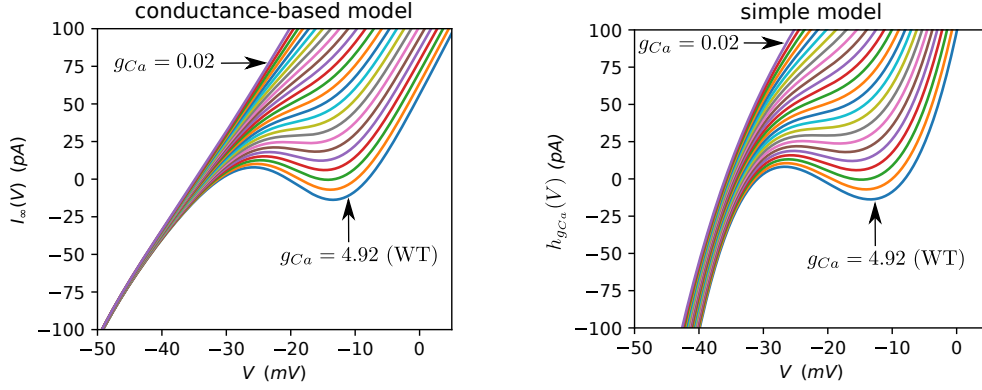


Figure 5: Comparison between the SSC of the CBM and the function h defined in (3) for a series of calcium conductance values g_{Ca} starting from 4.92nS (WT) and decreasing to 0.02nS by 0.2nS decrements.

240 The second implication stems from the perfect fitting of the function $h_{g_{Ca}}$ with the
 241 intermediate values of its associated SSC for any value of g_{Ca} (see Figure 6.A that exem-
 242 plifies this for $g_{Ca} = 4.82$ nS). For phenotypes 2 and 3, this implies that the voltage jumps
 243 between the down- and up-states of the neuron occur for the same values in the CBM as in
 244 the simple model for any value of g_{Ca} (Figure 6.B). That is, the saddle-node bifurcations in
 245 the CBM and in the simple model appear for the same values of injection current. Figure
 246 S5 shows a representative example (for $g_{Ca} = 4.82$ nS) of the voltage jump to its up-state
 247 in the CBM and in the simple model. In the same way, the CBM and the simple model
 248 relax to the same resting values for any value of g_{Ca} (Figure S6).

249 Furthermore, both in the CBM and in the simple model, we observe a loss of the overall
 250 voltage amplitude as g_{Ca} decreases (Figure 6.D), which is a paramount characteristic of the
 251 behavior of non-spiking neurons under the effect of calcium conductance decrease. This
 252 observation is partly due to the increase in voltage jump threshold values, as well as the
 253 decrease in resting potential values (Figure S6), both resulting from the decrease of g_{Ca} .

254 Finally, a relative deterioration of the fitting of the SSC for higher and lower values can
 255 be observed in Figure 6.A. Nonetheless, it should be noted that substantial noise in the
 256 recording of SSCs of non-spiking *C. elegans* neurons can be observed for extreme values, as
 257 in the bistable AFD neuron (Figure S7), which is similar to what we obtain (Figure 6.A).

258 Taken together, the aforementioned observations confirm that the main qualitative
 259 features of the raw neuron dynamics are accurately preserved by the simple model. From
 260 then on, it can be safely concluded that the simple model is adequate for the description
 261 of the neuron behavior as g_{Ca} evolves.

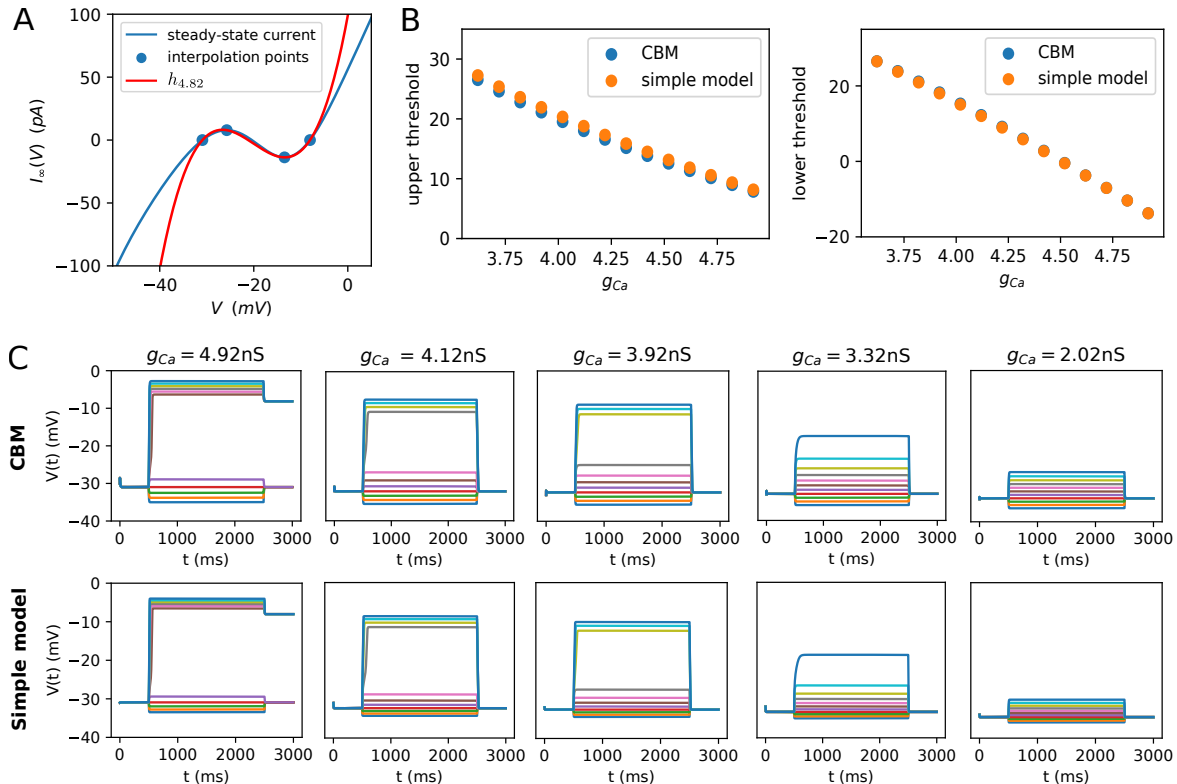


Figure 6: **(A)** Example of SSC ($g_{Ca} = 4.82\text{nS}$) of the CBM (in blue) against the function $h_{4.82}$ of the simple model (in red) defined in (3). **(B)** Upper and lower threshold of injection currents between the down- and up-states in the CBM and in the simple model. **(C)** Comparison of the voltage amplitude decrease in CBM and in the simple model.

5 Discussion

Summary. CBMs and ‘phenomenological’ models are often used to deal with distinct issues. CBMs are well suited to study ‘low-level’ functions of nervous systems, depending on physiological microscopic parameters such as ion conductances. Indeed, a CBM is a biophysical representation of a neuron in which every individual parameter and state variable has an established electrophysiological meaning. Nevertheless, the simulation of this type of model is very time-consuming, so the size of neural networks composed of CBMs that can be studied is inherently limited. In contrast, “phenomenological” models are very lightweight and simple so that one can simulate large-scale networks in real time. But their drawback is the lack of biophysical realism since it describes the macroscopic behavior of neurons regardless the underlying microscopic physiological processes. As a consequence, ‘phenomenological’ models exhibit dimensionless parameters and are therefore limited to the study of ‘higher-level’ functions of neural systems. This paper aimed to

275 propose a model for non-spiking neuron dynamics that combines the strengths of the two
276 types of models: the biological plausibility of CBMs with the high computational efficiency
277 of phenomenological models. To do this, a numerical procedure was proposed to establish
278 a relationship between the dimensionless parameters of a non-spiking phenomenological
279 model (Naudin et al., 2022b) and the ion conductances of CBMs or neurons. We applied
280 it to a model of an intrinsically non-spiking cell type, the retinal cone, associated with
281 a decrease in g_{Ca} . We showed that the resulting ‘conductance-based phenomenological
282 non-spiking model’ was able to accurately depict the phenotypic transitions of non-spiking
283 neurons as g_{Ca} evolves, previously described with CBMs (Naudin et al., 2022c). Therefore,
284 the resulting model combined the biological plausibility of CBMs with the high computa-
285 tional efficiency of phenomenological models, and thus may serve as a building block for
286 studying both ‘high-level’ and ‘low-level’ functions of non-spiking neural networks.

287 **Potential applications to the study of the effect of physiological and patho-**
288 **logical changes on non-spiking neural network dynamics.** Given the importance
289 of ion channels and ion flow for many physiological and pathological functions, both in
290 spiking and in non-spiking neurons, it could be valuable to have a direct relationship with
291 ion conductances when using phenomenological models. This would allow to study various
292 systems and nervous tissues, considering the physiological range of functioning, as well as
293 the pathological variations of their associated ion conductance. Our conductance-based
294 phenomenological non-spiking model was designed in this context, with a particular fo-
295 cus on the calcium conductance variations due to its crucial role in the electrical signal
296 generation in non-spiking neurons.

297 Indeed, non-spiking neurons, such as *C. elegans* neurons or retinal cells, exhibit a
298 variety of ion channels on their cell membrane, including many voltage-gated calcium and
299 calcium-gated potassium channels (Bargmann, 1998; Taylor et al., 2021; Van Hook et al.,
300 2019). The flow of ions in and out of the cells through these channels provides non-spiking
301 neurons with several crucial physiological properties, including their electrical activity.
302 In particular, voltage-gated calcium channels are essential in *C. elegans* which lacks the
303 voltage-gated Na^+ channels (Bargmann, 1998) that are usually involved in action potential
304 generation in vertebrates. Likewise, in many retinal cell classes including the cone, rod,
305 bipolar, horizontal and some amacrine cells, voltage-gated Na^+ channels are absent or
306 barely expressed, giving great importance to calcium channels in retinal electrical signal
307 generation (Van Hook et al., 2019). Therefore, it may be particularly relevant to have the
308 ability to assess the impact of calcium gradient variations on neuron behavior as well as
309 on network dynamics.

310 Furthermore, several mechanisms may alter the “normal” function of ion channels.
311 In particular, many studies show that mutations within genes encoding calcium channels
312 are often associated with various neurological and psychiatric diseases (Andrade et al.,
313 2019). Yet, these ion channels are ubiquitous in the retina cells, whose electrical activity is
314 disturbed as suggested by electrophysiological recordings (electroretinograms) conducted
315 in patients suffering from Parkinson’s, Alzheimer’s and Huntington’s diseases, epilepsy,
316 depression and schizophrenia (Silverstein et al., 2020). In this case, it would also be of
317 particular interest to gain insight into the levels of ion conductance that might lead to
318 pathological behavior.

319 Taken together, these information confirm that the use of the simple phenomenological
320 model, rather than CBMs, to address these issues is justified both by its minimal computa-
321 tional cost and by its biological plausibility. This original combination allows for the study
322 of precise physiological and pathological changes in a context of large-scale simulations of
323 the retina or *C. elegans* networks.

324 Acknowledgements

325 We thank Dr. Mellem and Dr. Liu for their consents to reproduce their experimental
326 data.

327 We thank the INS2I-CNRS and Loria for their financial support on the ModERN-Psy
328 project.

329 Code accessibility

330 The code used in this paper to build the conductance-based phenomenological non-spiking
331 model is available at:

332 <https://gitlab.com/lois76/article-procedure-cbm-phenomenological-model>.

333 Declaration of competing interests

334 The authors declare no competing interests.

Supplementary materials

Here we present the phenomenological model capable of reproducing the qualitative behaviors of non-spiking neurons, developed in [Naudin et al. \(2022b\)](#). In addition, we recall the role played by the steady-state current (SSC) in the dynamics of non-spiking neurons, since the numerical method developed in this paper fundamentally rely on it.

The phenomenological model

The phenomenological model, developed in [Naudin et al. \(2022b\)](#), is built on the basis of the bifurcation structure of conductance-based models of non-spiking neurons. For the convenience of reading the paper, we present it in this section.

Conductance-based models (CBMs). In CBMs, the dynamics of the membrane potential V is described by a general equation of the form

$$C \frac{dV}{dt} = - \sum_{ion} I_{ion} + I \quad (4)$$

where C is the membrane capacitance, $\sum_{ion} I_{ion}$ is the total current flowing across the cell membrane, and I is an applied current. The currents I_{ion} take the form

$$I_{ion} = g_{ion} m_{ion}^a h_{ion}^b (V - E_{ion})$$

where m (*resp.* h) denotes the probability for an activation (*resp.* inactivation) gate to be in the open state; a and b are the number of activation and inactivation gates, respectively; g_{ion} is the maximal conductance associated with ion ; and E_{ion} is the reversal potential.

Bifurcation dynamics of non-spiking CBMs. In non-spiking CBMs, the SSC curve I_{∞} determines the number of equilibria of the system and their values, as well as the bifurcations of the resting state along with the values to which they occur. It takes the general form

$$I_{\infty}(V) = \sum_{ion} I_{ion\infty}(V) \quad \text{where} \quad I_{ion\infty}(V) = g_{ion} m_{ion\infty}^a(V) h_{ion\infty}^b(V) (V - E_{ion}) \quad (5)$$

with

$$x_\infty(V) = \frac{1}{1 + \exp\left(\frac{V_{1/2}^x - V}{k_x}\right)}, \quad x \in \{m, h\}.$$

354 where $V_{1/2}^x$ and k_x are constant parameters.

355 Any stationary point of gating variables $x \in \{m, h\}$ must satisfy $x_* = x_\infty(V_*)$. Replacing
 356 this into the first equation on V , fixed points V_* of such models satisfy the equation

$$I_\infty(V_*) = I. \quad (6)$$

357 In other words, equilibria V_* correspond to the intersection between the SSC I_∞ and
 358 a horizontal line $I = c$ where c is a constant. There are two standard steady-state
 359 curves I_∞ , monotonic and cubic (Figure S1), each involving fundamentally different neuro-
 360 computational properties for non-spiking neurons:

- 361 • As shown in Figure S1.A, CBMs with a monotonic SSC only have one equilibrium
 362 for any value of I . Non-spiking neurons with such a SSC display a near-linear behav-
 363 ior characterized by smooth depolarizations or hyperpolarizations from the resting
 364 potential, such as the RIM neuron (Figure S2).
- 365 • As shown in Figure S1.B, a N-shaped curve leads to a saddle-node bifurcation. When
 366 $I = c_1$, there are 3 equilibria, noted $V_{1*}^{c_1}$, $V_{2*}^{c_1}$ and $V_{3*}^{c_1}$. Increasing I results in coa-
 367 lescence of two equilibria (the stable $V_{1*}^{c_1}$ with the unstable $V_{2*}^{c_1}$). The value $I = c_2$,
 368 at which the equilibria coalesce, is called the *bifurcation value*. For this value of I ,
 369 there exist 2 equilibria. For $I > c_2$, the system has only one equilibrium (*e.g.* $I = c_3$).
 370 In summary, when the parameter I increases, a stable and an unstable equilibrium
 371 approach, coalesce, and then annihilate each other. Non-spiking neurons with a N-
 372 shaped SSC display a bistable behavior characterized by a voltage jump between
 373 the resting potential and a depolarized potential of higher voltage, such as the AFD
 374 neuron (Figure S2).

375 Therefore, it can be stated that the SSC determines the bifurcation structure of non-
 376 spiking neurons and the equilibrium values of their graded responses to particular stimuli.

377 **The simple model.** Let V represent the membrane potential of a neuron. The simple
 378 model takes the general form

$$\tau \frac{dV}{dt} = -f(V) + I \quad (7)$$

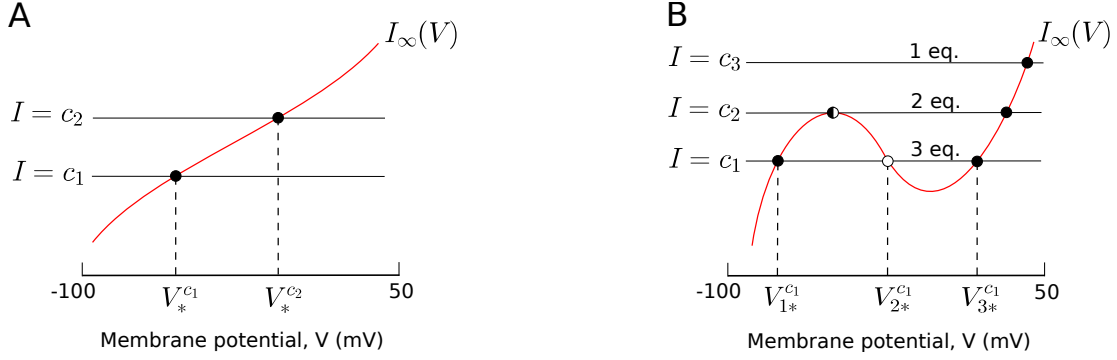


Figure S1: Two typical shapes of the SSC $V \rightarrow I_\infty(V)$, in red. Intersections of I_∞ and horizontal line $I = c$ (with c constant) correspond to equilibria of the system. We denote stable equilibria as filled circles ●, unstable equilibria as open circles ○ and saddle-node equilibria as ◐. **(A)** Monotonic SSC. $V_*^{c_1}$ and $V_*^{c_2}$ correspond to equilibria for a current injection $I = c_1$ and $I = c_2$ respectively. **(B)** N-shaped SSC. The number of equilibria of the system depends on the value of I . For the sake of readability, we highlight equilibria only for $I = c_1$, noted $V_{1*}^{c_1}$, $V_{2*}^{c_1}$ and $V_{3*}^{c_1}$.

379 with f a cubic function which reads as

$$f(V) = aV^3 + bV^2 + cV + d. \quad (8)$$

The function f plays the same role in the dynamics of the model (7) as the SSC I_∞ in CBMs (4). Indeed, fixed points V_* of model (7) satisfy

$$f(V_*) = I$$

380 so that the shape of f determines the neuro-computational features of the non-spiking
 381 model: a monotonic shape involves a near-linear behavior of the model, while a N-shape
 382 implies a bistable one with the occurrence of two saddle-node bifurcations. Therefore, the
 383 model proposes a simple cubic expression (8) that plays the same role as the complex SSC
 384 expression (5) of CBMs. Parameters a , b , c and d are dimensionless and are estimated in
 385 order to fit the experimental SSC. Parameter τ describes the *constant* time for which V
 386 reaches its equilibrium value V_* . This parameter can be either hand-tuned or estimated
 387 from experimental voltage.

388 Conductance-based model of the retinal cone

389 The conductance-based model of the canonical bistable cell is based on the retinal cone
 390 cell built in Kourennyi et al. (2004). It has four ion currents: a calcium current (I_{Ca}), a
 391 hyperpolarization-activated current (I_h), a delayed rectifying potassium current (I_{Kv}), and
 392 a leak current (I_L). The parameters are expressed in the following units: mV (voltage),
 393 pA (current), nS (conductance), and ms (time). The membrane capacitance (C) is set
 394 to 16 nF. We denote by g_{ion} the maximal conductance (namely the conductance of the
 395 channel when all the gates are open), and E_{ion} the reversal potential, that is, the potential
 396 at which the ion current reverses its direction. Leak current is classically described as
 397 $I_L = g_L(V - E_L)$ and the remaining currents are described in Table S1.

Ion current (I_{ion})	$\alpha_{ion}(V)$ and $\beta_{ion}(V)$ rates	g_{ion} and E_{ion}
$I_{Ca} = g_{Ca}m_{Ca}h_{Ca}(V - E_{Ca})$ $\frac{dm_{Ca}}{dt} = \alpha_{Ca}(1 - m_{Ca}) - \beta_{Ca}m_{Ca}$	$\alpha_{Ca}(V) = 3.1 e^{(V+16.6)/11.4}$ $\beta_{Ca}(V) = 3.1 e^{(-V-16.6)/11.4}$	$g_{Ca} = 4.92$ $E_{Ca} = 40$
$I_h = g_h(1 - (1 + 3m_h)(1 - m_h)^3)(V - E_h)$ $\frac{dm_h}{dt} = \alpha_{m_h}(1 - m_h) - \beta_{m_h}m_h$	$\alpha_{m_h}(V) = \frac{18}{(1 + e^{(V+88)/12})}$ $\beta_{m_h}(V) = \frac{18}{(1 + e^{-(V+18)/19})}$	$g_h = 3.5$ $E_h = -32.5$
$I_{Kv} = g_{Kv}m_{Kv}^3h_{Kv}(V - E_K)$ $\frac{dm_{Kv}}{dt} = \alpha_{m_{Kv}}(1 - m_{Kv}) - \beta_{m_{Kv}}m_{Kv}$ $\frac{dh_{Kv}}{dt} = \alpha_{h_{Kv}}(1 - h_{Kv}) - \beta_{h_{Kv}}h_{Kv}$	$\alpha_{m_{Kv}}(V) = \frac{5(V - 100)}{(1 - e^{-(V-100)/42})}$ $\beta_{m_{Kv}}(V) = 9e^{(20-V)/40}$ $\alpha_{h_{Kv}}(V) = 0.15e^{-V/22}$ $\beta_{h_{Kv}}(V) = \frac{0.4125}{(1 + e^{(10-V)/7})}$	$g_{Kv} = 2$ $E_{Kv} = -80$

Table S1: Summary of ion currents composing the generic bistable model.

398 **Supplementary figures**

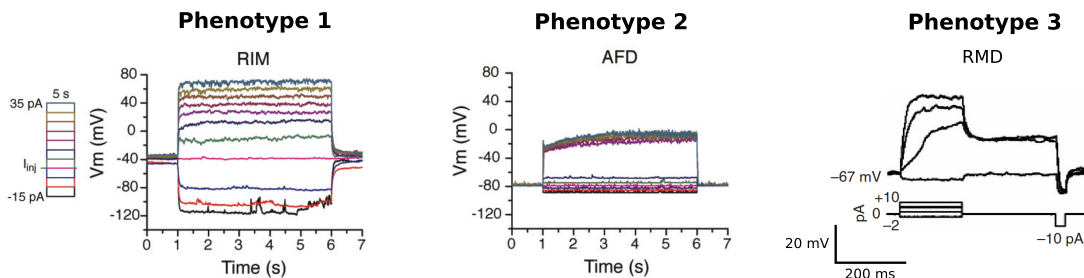


Figure S2: Experimental voltage examples from *C. elegans* of each phenotype for a series of current injections starting from -15pA and increasing to 35pA by 5pA increments for the RIM and AFD neurons, and starting from -2pA and increasing to 10pA by 3pA increments for the RMD neuron. Phenotype 1 refers to near-linear neurons, phenotype 2 to bistable neurons with one resting potential, and phenotype 3 to bistable neurons with two resting potentials. The experimental data of the RIM and AFD neurons have been reproduced from [Naudin et al. \(2022a\)](#), and from [Mellem et al. \(2008\)](#) for the RMD neuron with the consent of the authors.

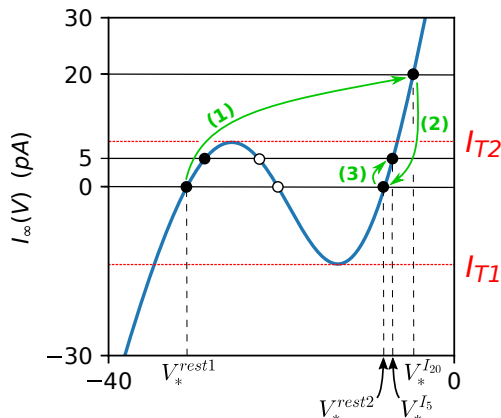


Figure S3: Diagram explaining the short-term memory capacity of a neuron with a phenotype 3. I_{T1} (resp. I_{T2}) denotes the injection current thresholds at which the neuron jumps to its upper (resp. lower) voltage plateau. (1) A brief transient stimulus ($20 > I_{T2}$ pA) is applied and the voltage converges to V_*^{I20} . (2) The stimulus ceases so that the voltage relaxes to V_*^{rest2} which is the new voltage initial condition. (3) A new depolarizing current step (5pA) is applied and the voltage goes to V_{2*}^{I5} and not V_{1*}^{I5} since V_*^{rest2} now belongs to the basin of attraction of V_{2*}^{I5} . This figure has been reproduced from [Naudin et al. \(2022c\)](#) with the consent of the authors.

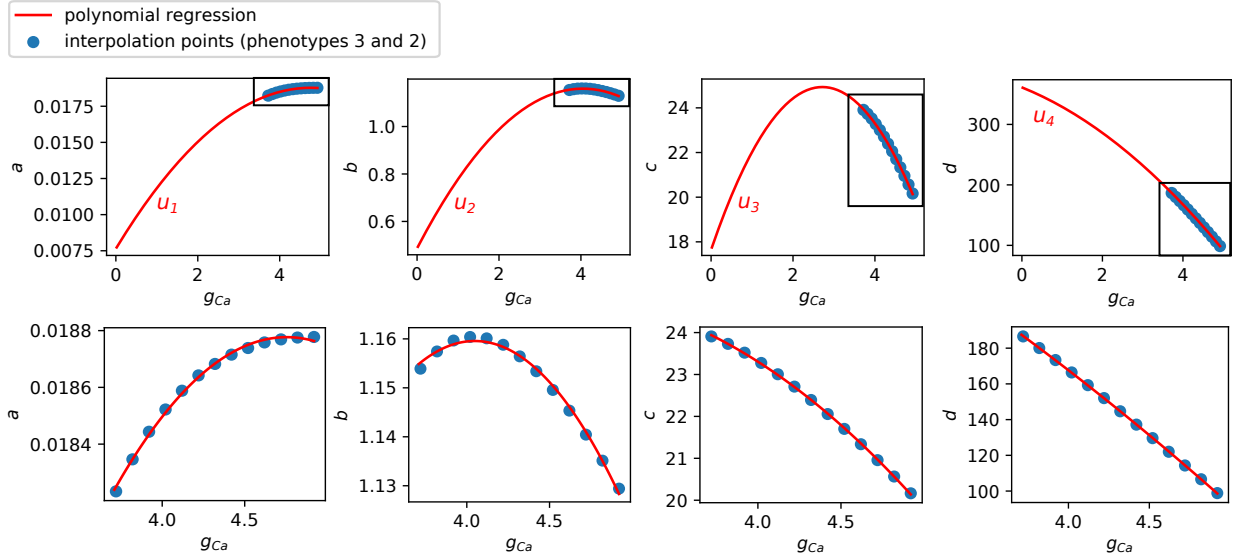


Figure S4: **(Top)** Two-degree polynomials u_i , $i = 1, \dots, 4$, built from the polynomial regression of blue points. These points are generated following Step 1 and Step 2 of the procedure described in Section 3. **(Bottom)** Zoom of the rectangles in (Top).

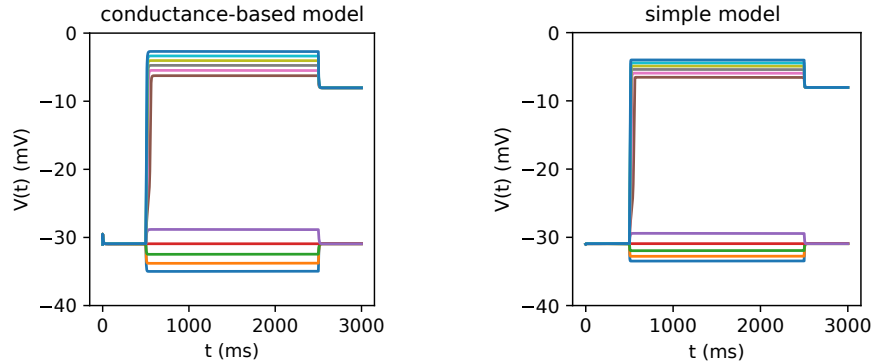


Figure S5: Comparison of voltage dynamics between CBM and the conductance-based phenomenological non-spiking model for $g_{Ca} = 4.82\text{nS}$ for a series of injection currents starting from -15pA and increasing to 35pA by 5pA increments.

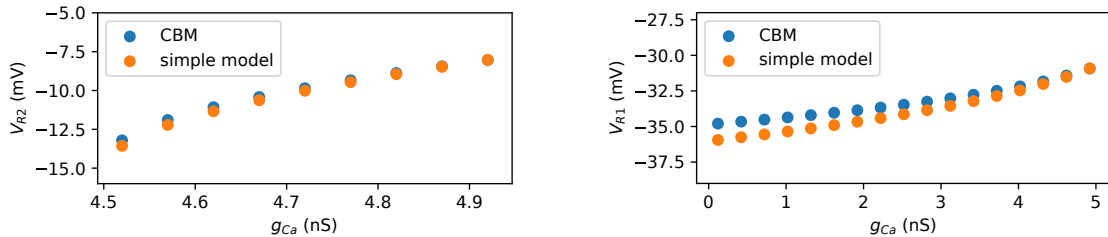


Figure S6: Comparison of the resting potential values (V_{R1} and V_{R2}) for various values of g_{Ca} in the CBM and in the simple model.

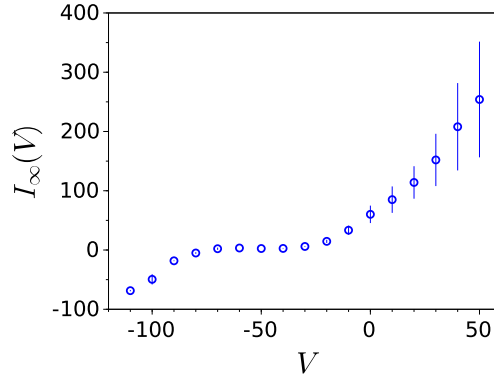


Figure S7: SSC of the AFD neuron obtained from averaged voltage-clamp recordings ($n = 3$) (Liu et al., 2018).

References

- 399
- 400 A. Andrade, A. Brennecke, S. Mallat, J. Brown, J. Gomez-Rivadeneira, N. Czepiel, and
 401 L. Londrigan. Genetic associations between voltage-gated calcium channels and psychi-
 402 atric disorders. *International journal of molecular sciences*, 20(14):3537, 2019.
- 403 T. Aoyama, Y. Kamiyama, S. Usui, R. Blanco, C. F. Vaquero, and P. de la Villa. Ionic
 404 current model of rabbit retinal horizontal cell. *Neuroscience Research*, 37(2):141–151,
 405 2000.
- 406 J. Art and M. Goodman. Ionic conductances and hair cell tuning in the turtle cochlea a.
 407 *Annals of the New York Academy of Sciences*, 781(1):103–122, 1996.
- 408 C. I. Bargmann. Neurobiology of the caenorhabditis elegans genome. *Science*, 282(5396):
 409 2028–2033, 1998.
- 410 S. S. Bidaye, T. Bockemühl, and A. Büschges. Six-legged walking in insects: how cpgs,
 411 peripheral feedback, and descending signals generate coordinated and adaptive motor
 412 rhythms. *Journal of neurophysiology*, 119(2):459–475, 2018.
- 413 R. Brette. What is the most realistic single-compartment model of spike initiation? *PLoS*
 414 *computational biology*, 11(4):e1004114, 2015.
- 415 M. Burrows, G. Laurent, and L. Field. Proprioceptive inputs to nonspiking local interneu-
 416 rons contribute to local reflexes of a locust hindleg. *Journal of Neuroscience*, 8(8):
 417 3085–3093, 1988.

- 418 R. Davis and A. Stretton. Passive membrane properties of motorneurons and their role in
419 long-distance signaling in the nematode ascaris. *Journal of Neuroscience*, 9(2):403–414,
420 1989a.
- 421 R. E. Davis and A. Stretton. Signaling properties of ascaris motorneurons: graded ac-
422 tive responses, graded synaptic transmission, and tonic transmitter release. *Journal of*
423 *Neuroscience*, 9(2):415–425, 1989b.
- 424 C. Eliasmith and O. Trujillo. The use and abuse of large-scale brain models. *Current*
425 *opinion in neurobiology*, 25:1–6, 2014.
- 426 G. B. Ermentrout and D. H. Terman. *Mathematical foundations of neuroscience*, volume 35.
427 Springer Science & Business Media, 2010.
- 428 R. Fettilplace. Electrical tuning of hair cells in the inner ear. *Trends in Neurosciences*, 10
429 (10):421–425, 1987.
- 430 G. D. Field and E. Chichilnisky. Information processing in the primate retina: circuitry
431 and coding. *Annu. Rev. Neurosci.*, 30:1–30, 2007.
- 432 R. FitzHugh. Impulses and physiological states in theoretical models of nerve membrane.
433 *Biophysical journal*, 1(6):445–466, 1961.
- 434 F. Giovannini, B. Knauer, M. Yoshida, and L. Buhry. The can-in network: A biologi-
435 cally inspired model for self-sustained theta oscillations and memory maintenance in the
436 hippocampus. *Hippocampus*, 27(4):450–463, 2017.
- 437 M. B. Goodman, D. H. Hall, L. Avery, and S. R. Lockery. Active currents regulate sensi-
438 tivity and dynamic range in *c. elegans* neurons. *Neuron*, 20(4):763–772, 1998.
- 439 T. Górski, D. Depannemaecker, and A. Destexhe. Conductance-based adaptive exponential
440 integrate-and-fire model. *Neural Computation*, 33(1):41–66, 2021.
- 441 A. L. Hodgkin and A. F. Huxley. A quantitative description of membrane current and its
442 application to conduction and excitation in nerve. *The Journal of physiology*, 117(4):
443 500–544, 1952.
- 444 S. W. Hughes, D. W. Cope, T. I. Tóth, S. R. Williams, and V. Crunelli. All thalamo-
445 cortical neurones possess a t-type ca^{2+} ‘window’ current that enables the expression of
446 bistability-mediated activities. *The Journal of physiology*, 517(3):805–815, 1999.

- 447 E. M. Izhikevich. Simple model of spiking neurons. *IEEE Transactions on neural networks*,
448 14(6):1569–1572, 2003.
- 449 E. M. Izhikevich. Which model to use for cortical spiking neurons? *IEEE transactions on*
450 *neural networks*, 15(5):1063–1070, 2004.
- 451 D. E. Kourennyi, X.-d. Liu, J. Hart, F. Mahmud, W. H. Baldrige, and S. Barnes. Recip-
452 rocal modulation of calcium dynamics at rod and cone photoreceptor synapses by nitric
453 oxide. *Journal of neurophysiology*, 92(1):477–483, 2004.
- 454 P. E. Latham, B. Richmond, P. Nelson, and S. Nirenberg. Intrinsic dynamics in neuronal
455 networks. i. theory. *Journal of neurophysiology*, 83(2):808–827, 2000.
- 456 G. Laurent and M. Burrows. Intersegmental interneurons can control the gain of reflexes in
457 adjacent segments of the locust by their action on nonspiking local interneurons. *Journal*
458 *of Neuroscience*, 9(9):3030–3039, 1989.
- 459 L. Lemaire, M. Desroches, M. Krupa, L. Pizzamiglio, P. Scalmani, and M. Mantegazza.
460 Modeling nav1. 1/scn1a sodium channel mutations in a microcircuit with realistic ion
461 concentration dynamics suggests differential gabaergic mechanisms leading to hyper-
462 excitability in epilepsy and hemiplegic migraine. *PLoS Computational Biology*, 17(7):
463 e1009239, 2021.
- 464 Q. Liu, P. B. Kidd, M. Dobosiewicz, and C. I. Bargmann. *C. elegans* awa olfactory neurons
465 fire calcium-mediated all-or-none action potentials. *Cell*, 175(1):57–70, 2018.
- 466 S. R. Lockery, M. B. Goodman, and S. Faumont. First report of action potentials in a *c.*
467 *elegans* neuron is premature. *Nature neuroscience*, 12(4):365–366, 2009.
- 468 J. E. Mellem, P. J. Brockie, D. M. Madsen, and A. V. Maricq. Action potentials contribute
469 to neuronal signaling in *c. elegans*. *Nature neuroscience*, 11(8):865–867, 2008.
- 470 L. Naudin. Biological emergent properties in non-spiking neural networks. *AIMS Mathe-*
471 *matics*, 7(10):19415–19439, 2022.
- 472 L. Naudin, J. L. Jiménez Laredo, Q. Liu, and N. Corson. Systematic generation of bio-
473 physically detailed models with generalization capability for non-spiking neurons. *PloS*
474 *one*, 17(5):e0268380, 2022a.
- 475 L. Naudin, J. L. J. Laredo, and N. Corson. A simple model of non-spiking neurons. *Neural*
476 *Computation*, 34(10), 2022b.

- 477 L. Naudin, L. Raison-Aubry, and L. Buhry. General pattern of non-spiking neuron dy-
478 namics under the effect of potassium and calcium channel modifications. *Under review*,
479 2022c.
- 480 M. Nicoletti, A. Loppini, L. Chiodo, V. Folli, G. Ruocco, and S. Filippi. Biophysical
481 modeling of *c. elegans* neurons: Single ion currents and whole-cell dynamics of *awcon*
482 and *rmd*. *PloS one*, 14(7):e0218738, 2019.
- 483 T. O’Leary, A. C. Sutton, and E. Marder. Computational models in the age of large
484 datasets. *Current opinion in neurobiology*, 32:87–94, 2015.
- 485 P. Poirazi and A. Papoutsis. Illuminating dendritic function with computational models.
486 *Nature Reviews Neuroscience*, pages 1–19, 2020.
- 487 A. Roberts and B. M. Bush. *Neurones without impulses: their significance for vertebrate*
488 *and invertebrate nervous systems*, volume 6. Cambridge University Press, 1981.
- 489 S. M. Silverstein, D. L. Demmin, J. B. Schallek, and S. I. Fradkin. Measures of reti-
490 nal structure and function as biomarkers in neurology and psychiatry. *Biomarkers in*
491 *Neuropsychiatry*, 2:100018, 2020.
- 492 G. D. Smith, C. L. Cox, S. M. Sherman, and J. Rinzel. Fourier analysis of sinusoidally
493 driven thalamocortical relay neurons and a minimal integrate-and-fire-or-burst model.
494 *Journal of neurophysiology*, 83(1):588–610, 2000.
- 495 S. R. Taylor, G. Santpere, A. Weinreb, A. Barrett, M. B. Reilly, C. Xu, E. Varol,
496 P. Oikonomou, L. Glenwinkel, R. McWhirter, et al. Molecular topography of an en-
497 tire nervous system. *Cell*, 184(16):4329–4347, 2021.
- 498 S. Usui, A. Ishihaiza, Y. Kamiyama, and H. Ishii. Ionic current model of bipolar cells in
499 the lower vertebrate retina. *Vision research*, 36(24):4069–4076, 1996.
- 500 M. J. Van Hook, S. Nawy, and W. B. Thoreson. Voltage- and calcium-gated ion channels of
501 neurons in the vertebrate retina. *Progress in retinal and eye research*, 72:100760, 2019.
- 502 S. R. Williams, T. I. Toth, J. P. Turner, S. W. Hughes, and V. Crunelli. The ‘win-
503 dow’ component of the low threshold ca^{2+} current produces input signal amplification
504 and bistability in cat and rat thalamocortical neurones. *The Journal of physiology*, 505
505 (3):689–705, 1997.